Two-dimensional local density of states in two-dimensional photonic crystals

Ara A. Asatryan,[1] Sebastien Fabre,[1] Kurt Busch,[2] Ross C. McPhedran,[1] Lindsay C. Botten,[3] C. Martijn de Sterke,[1] Nicolae-Alexandru P. Nicorovici.[1]

1: School of Physics, University of Sydney, NSW 2006, Australia

2: Institut für Theorie der Kondensierten Materie, University of Karlsruhe P.O. Box 6980, 76128 Karlsruhe, Germany

3: School of Mathematical Sciences, University of Technology, Sydney, N.S.W. 2007, Australia

ara@physics.usyd.edu.au

Abstract: We calculate the two-dimensional local density of states (LDOS) for two-dimensional photonic crystals composed of a finite cluster of circular cylinders of infinite length. The LDOS determines the dynamics of radiation sources embedded in a photonic crystal. We show that the LDOS decreases exponentially inside the crystal for frequencies within a photonic band gap of the associated infinite array and demonstrate that there exist "hot" and "cold" spots inside the cluster even for wavelengths inside a gap, and also for wavelengths corresponding to pass bands. For long wavelengths the LDOS exhibits oscillatory behavior in which the local density of states can be more than 30 times higher than the vacuum level.

OCIS codes: (050.0050), Diffraction grating, (290.4210) Scattering

References and links

1. E. Yablonovitch, "Inhibited Spontaneous Emission in Solid-State Physics and Electronics," Phys. Rev. Lett. **58**, 2059-2062 (1987).
2. S. John, "Strong Localization of Photons in Certain Disordered Dielectric Superlattices," Phys. Rev. Lett. **58**, 2486-2489 (1987).
3. K. Busch, and S. John,"Liquid-Crystal Photonic-Band-Gap Materials: The Tunable Electromagnetic Vacuum," Phys. Rev. Lett. **83**, 967-970 (1999).
4. O. Painter, R.K. Lee, A. Scherer, A. Yariv, J. D. O'Brien, P.D. Dapkus, and I. Kim, "Two-Dimensional Photonic Band-Gap Defect Mode Laser," Science **284**, 1819-1821 (1999).
5. S. Fan, and J.D. Joannopoulos,"Photonic crystals: towards large-scale integration of optical and optoelectronic circuits," Optics & photonics news, **11** 28-33 (2000).
6. J. C. Knight, J. Broeng, T. A. Birks, and P. St. J. Russel, "Photonic Band Gap Guidance in Optical Fibers," Science **282**, 1476-1478 (1998)
7. R. Spirk, B. A. van Tiggelen, A. Lagendijk, "Optical emission in periodic dielectrics," Europhys. Lett. **35**, 265-270 (1996).
8. S. John, and K. Busch , "Photonic bandgap formation and tunability in certain self-organizing systems," J. Lightwave Technology **17**, 1931-1943 (1999).
9. A. Moroz,"Minima and maxima of the local density of states for one-dimensional periodic systems," Europhys. Lett. **46**, 419-424 (1999).
10. G.S. Agarwal,"Quantum electrodynamics in the presence of dielectrics and conductors. Parts I-III." Phys. Rev. A, **11**, 230-264 (1975).
11. A. A. Asatryan, K. Busch, R. C. McPhedran, L.C. Botten, C. Martijn de Sterke, and N. A. Nicorovici, "Two-dimensional Green function and local density of states in photonic crystals consisting of a finite number of cylinders of infinite length", Phys. Rev. E submitted.

#27699 - $15.00 US
Received November 13, 2000; Revised January 09, 2001

12. J. M. Bendickson, J. P. Dowling, and M. Scalora, "Analytic expressions for the electromagnetic mode density in finite, one-dimensional, photonic band-gap structures", Phys. Rev. E **53**, 4107–4121 (1996).
13. H. Kosaka, T. Kawashima, A. Tomita, M. Notomi, T. Tamamura, T. Sato, and S. Kawakami, "Superprism phenomena in photonic crystals", Phys. Rev. B **58**, 10096–10099 (1998).
14. B. Gralak, S. Enoch, and G. Tayeb, "Anomalous refractive properties of photonic crystals", J. Opt. Soc. Am. A **17**, 1012–1020 (2000).
15. J. D. Joanopoulos, R. D. Meade and J. N. Winn, "Photonic Crystals: Molding the Flow of Light," Princeton University Press. Princeton, NJ, 1995).

Photonic crystals were introduced by Yablonovitch [1] and John [2] and now constitute a mature research field in contemporary optics. In such materials, the spatial variation of dielectric constant prohibits the propagation of light for certain bands of frequencies and applications of such high-technology materials have already emerged. These include optical switches [3], microscopic lasers [4], the promise of large-scale optoelectronic integrated circuits [5], and optical fibers with photonic crystal cores [6].

Up until now, both the theoretical and experimental characterization of finite-sized structures have been concerned largely with the analysis of transmission and reflection spectra and the computation of band structure diagrams. However, a key point raised in both pioneering papers [1, 2] concerned radiation dynamics and the influence of photonic crystals on the density of states. Of particular interest is the variation with both frequency and spatial position that is encapsulated in the Local Density of States (LDOS). The LDOS determines the radiation dynamics of fluorescent sources embedded in photonic crystals [7] and, despite its status as one of the key quantities characterizing this behaviour, it has been calculated previously for only a few isolated positions in infinite 3D photonic crystals [8], and in the 1D case [9].

Here, we present results for the 2D Green's tensor and the LDOS for 2D photonic crystals composed of a finite cluster of circular cylinders (for both fundamental polarizations). We investigate the behaviour (see the attached Quicktime videos) of the LDOS as a function of wavelength as we cross the band gap of the associated infinite array, and highlight the presence of points of enhanced LDOS, particularly evident for frequencies near the edge of a band gap.

The LDOS ($\rho(\mathbf{r},\omega)$) is calculated from the electric Green's tensor $\mathbf{G}^e$ according to [10]

$$\rho(\mathbf{r};\omega) = -\frac{2\omega}{\pi c^2}\mathrm{Im}\mathrm{Tr}[\mathbf{G}^{\mathbf{e}}(\mathbf{r},\mathbf{r};\omega)]. \tag{1}$$

Here, $\mathbf{G}^e(\mathbf{r},\mathbf{r}_s;\omega)$ is the 3×3 electric field Green's tensor at the field position $\mathbf{r}$ corresponding to a current source at $\mathbf{r}_s$ of frequency ω. Each column of $\mathbf{G}^e$ represents the components of an electric field vector $[G^e_{xu}, G^e_{yu}, G^e_{zu}]$ generated by a source radiating parallel to the $u = x, y, z$ axes respectively. For a 2D in-plane problem, the polarizations decouple and the fields are specified by a single, longitudinal components: $V = E_z$ in the case of TM or $E_{\shortparallel}$ polarization, and by $V = H_z$ for TE of $H_{\shortparallel}$ polarization. For TM polarization, $G^e_{zz} = V_z$ is determined directly by the the solution of

$$\left(\nabla^2 + k^2 n^2(\mathbf{r})\right) V_z(\mathbf{r}) = \delta(\mathbf{r}-\mathbf{r}_s), \tag{2}$$

associated with a monopole source. Here, $n(\mathbf{r})$ denotes the refractive index. For TE polarization, the process is less direct and requires the solution of two scalar problems for $V^u_z = H_z$ satisfying

$$\left(\nabla^2 + k^2 n^2(\mathbf{r})\right) V^u_z(\mathbf{r}) = -i\widehat{\mathbf{z}}\cdot[\nabla\times\mathbf{u}\,\delta(\mathbf{r}-\mathbf{r}_s)]/k, \tag{3}$$

respectively corresponding to a dipole source oriented in the directions $\mathbf{u} = \hat{x}, \hat{y}$. Here,

#27699 - $15.00 US
Received November 13, 2000; Revised January 09, 2001

$\mathbf{G}^e$ is characterized by a 2×2 tensor the elements of which are calculated according to $(G_{xu}, G_{yu}) = -i(\hat{\mathbf{z}} \times \nabla V_x^u)/(kn^2)$.

The clusters that we consider consist of N_c parallel, non-overlapping dielectric cylinders of radii a_l, refractive indices n_l, centered at positions $\mathbf{c}_l$ in a medium with refractive index $n_b = 1$. More details of the method are given in [11] and here we outline the approach, focusing on its attractive computational features. In the vicinity of the l^{th} cylinder, we expand fields in *local coordinates* (r_l, θ_l) with origin at $\mathbf{c}_l$ to facilitate the imposition of boundary conditions. For either polarization, V is expressed in exterior $r_l > a_l$ and interior $r_l < a_l$ multipole expansions

$$V(\mathbf{r}_l) = \begin{cases} \sum_{m=-\infty}^{\infty} \left[A_m^l J_m(kr_l) + B_m^l H_m^{(1)}(kr_l) \right] e^{im\theta_l}, \\ \\ \sum_{m=-\infty}^{\infty} \left[C_m^l J_m(kn_l r_l) + D_m^l H_m^{(1)}(kn_l r_l) \right] e^{im\theta_l}, \end{cases} \tag{4}$$

and a similar expression relating $\mathbf{C}$ with $\mathbf{B}$ and $\mathbf{D}$. Note that the terms with the D coefficients are associated with possible interior sources. In vector notation, with $\mathbf{B}^l = [B_m^l]$ denoting a vector of field source coefficients (with similar definitions for $\mathbf{A}$ and $\mathbf{D}$), we may express the boundary conditions in terms of cylindrical harmonic reflection $\mathbf{R}^l = [R_n^l]$ and transmission $\mathbf{T}^l = [T_n^l]$ coefficients

$$\mathbf{B}^l = \mathbf{R}^l \mathbf{A}^l + \mathbf{T}^l \mathbf{D}^l. \tag{5}$$

The coefficients $\mathbf{B}^l$ are determined from the field identity (6)that expresses the regular part of the field ($\mathbf{A}^l$) in terms of fields scattered by all other cylinders ($\mathbf{B}^j$, $j \neq l$) and real sources associated with the source terms arising in the wave equations. The field identity, whose derivation is given elsewhere [11], reduces to the partitioned system

$$\mathbf{B}^l - \mathbf{R}^l \sum_{j \neq l} \mathbf{S}^{lj} \mathbf{B}^j = \mathbf{R}^l \mathbf{Q}^l + \mathbf{T}^l \mathbf{K}^l \tag{6}$$

after applying the boundary conditions (5). In (6), the elements of the $\mathbf{S}^{lj}$ characterize the multipole contributions due to sources associated with each scatterer (and follow from Graf's addition theorem for Bessel functions), while the elements of $\mathbf{Q}^l$ and $\mathbf{K}^l$ are the multipole coefficients of the real, external and internal sources, respectively. The Green's function is then formed from the exterior form and the interior (for cylinder l) form of V:

$$V(\mathbf{r}, \mathbf{r}_s) = \begin{cases} \chi^{\text{ext}}(\mathbf{r}, \mathbf{r}_s) V_0(\mathbf{r}, \mathbf{r}_s) + \sum_{l=1}^{N_c} \sum_{m=-\infty}^{\infty} B_m^l H_m^{(1)}(kr_l)\, e^{im\theta_l}, \\ \\ \chi^{\text{int}}(\mathbf{r}_l, \mathbf{r}_s) V_0(\mathbf{r}, \mathbf{r}_s) + \sum_{m=-\infty}^{\infty} C_m^l J_m(kn_l r_l) e^{im\theta_l}. \end{cases} \tag{7}$$

In (7), V_0 is the solution of the field problem in the absence of scatterers and, for TM polarization, is given by $G_0 = H_0^{(1)}(kn|\mathbf{r} - \mathbf{r}_s|)/(4i)$, the Green's function for a homogeneous medium of refractive index $n = n_b$ and $n = n_l$ in the exterior and interior forms respectively. The χ^{ext} and χ^{int} are switch functions, with $\chi^{\text{ext}}(\mathbf{r}, \mathbf{r}_s) = 1$ for a source exterior to all cylinders, $\chi^{\text{int}}(\mathbf{r}_l, \mathbf{r}_s) = 1$ for a source interior to cylinder l, and vanishing for all other source locations. The accuracy of the method is governed by the number of terms that are retained in the field expansions (4). All calculations below have relative accuracies better than 10^{-4}, requiring 11 basis functions (i.e. $m \in [-5, 5]$) in the field expansions. For the general case, in which the refractive index of the background (n_b) differs from unity, the solution may be obtained from (7) by rescaling the wave number $k \to kn_b$ and the refractive indices of the cylinders $n_l \to n_l/n_b$.

#27699 - $15.00 US
Received November 13, 2000; Revised January 09, 2001

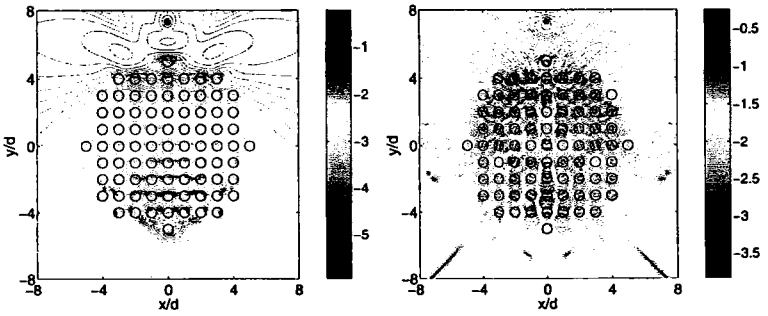

Fig. 1. Plot of $\log_{10}|G|$ for a wavelength in the gap $\lambda/d = 3.5$ (left panel) and in the pass band $\lambda/d = 2.5$ (right panel). The black dotes indicate the positions of the source which have coordinates $(0, 7.3)$ and the black circles indicate the cylinders.

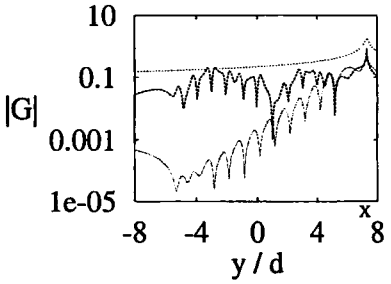

Fig. 2. Sections through Fig. 1 at $x = 0$: green line for $\lambda/d = 3.5$, blue line for $\lambda/d = 2.5$. The red line is the Green function for a line source without scatterers for $\lambda/d = 3.5$. The position of the source is indicated as x.

The multipole method that we are using has a number of significant advantages. First, its form facilitates the separation of the divergent real part of the Green's function at $\mathbf{r} = \mathbf{r_s}$ from the finite imaginary part that determines the LDOS (1). Secondly, the analytic imposition of boundary conditions at cylinder surfaces implies that the numerical problems, associated with high refractive index contrast (e.g. as may occur with metallic cylinders), that normally afflicts plane wave methods do not trouble this technique. Also, the computation of the spatial distribution of the LDOS for a given frequency and polarization requires only a single matrix inversion. This is because the coefficient matrix of (6) depends only on the relative placement of the cylinders, while dependence on the absolute positions of the source and field points is restricted to the right hand sides of the system. Thus, LDOS distributions may be calculated for many cylinders, at large numbers of field points, without incurring inordinately large computation times on workstations. Finally, we note than an effective DOS may be defined by averaging the LDOS over one or more central unit cells within the finite cluster. This DOS is non-zero within the band gap, since it corresponds to a finite sample, rather than a crystal of infinite extent, and thus can be used to investigate scaling of the DOS with sample size, and related questions.

In our numerical calculations we take all cylinders to have the same radius a and refractive index n_c, although we stress that neither restriction is necessary. The cylinders, with $n_c = 3$, are arranged in a square lattice with period d and normalized radius $a/d = 0.3$, corresponding to an area fraction of 28.3 percent. The corresponding infinite structure for TM polarization has a band gap for $2.986 < \lambda/d < 3.771$.

Fig. 1 displays the Green's function for a TM polarized wave field produced by a

#27699 - $15.00 US
Received November 13, 2000; Revised January 09, 2001

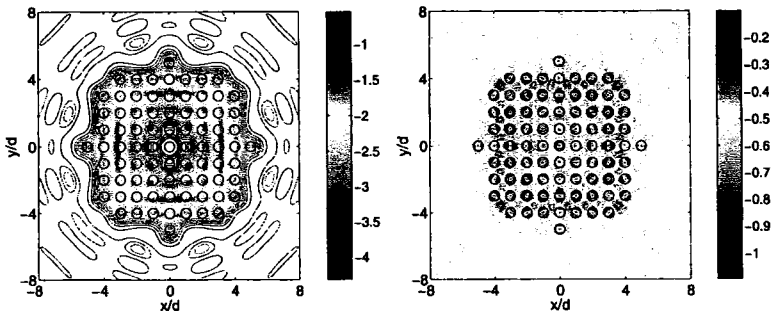

Fig. 3. $\log_{10}(\rho\pi c^2/2\omega)$ for TM polarization for $\lambda/d = 3.5$ (left panel) and for $\lambda/d = 2.5$ (right panel).

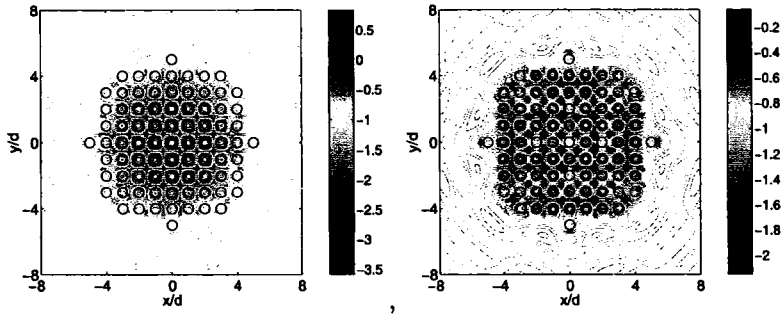

Fig. 4. $\log_{10}(\rho\pi c^2/2\omega)$ for TM polarization for $\lambda/d = 3.816$ with enhanced emission inside the cylinders (left panel), and for $\lambda/d = 4.11$ with enhanced emission in some of the cylinders.

source at $(x_s, y_s) = (0, 7.3)$ radiating into a cluster of $N_c = 81$ cylinders, while Fig. 2 shows a section of Fig. 1 along the line $x = 0$. For a wavelength in the gap (left panel, Fig. 1), the field decreases exponentially into the crystal, while in the pass band there is no such behavior. Note the divergence of the magnitude of the Green's function (associated with the singularity of its real part) at the source point. Also note that in the pass band, the Green's function has pronounced interference minima (Fig. 2), but in general oscillates about a trend line that is relatively flat.

Figure 3 shows the LDOS for gap and pass band wavelengths and corresponds to the LDOS data from two frames of the accompanying video clips. In the videos, each frame shows a contour map of the LDOS, the band diagram (with the frequency marked) for the corresponding infinite array, and a numerical display of the free space wavelength. Each of the three videos shows a different view of the LDOS map—from below, above and the side—in order to display clearly the regions of suppressed (below) and enhanced emission (above, side). Figs 3 and 4 correspond to views from above.

The most striking features in the video clips concern the development of a region of suppressed emission within the band gap, and the flashes of enhanced emission for particular wavelengths on either side of the gap. A similar result has been observed in 1D [12] and may be related to the super-prism and ultra-refraction effects [13, 14] caused by strong changes in the group velocity in the vicinity of a band edge.

The left panel of Fig. 4 shows strongly enhanced emission for all cylinders in the sample, apart from those in the edge layer. For the point with coordinates $(0, 0.2)$ the LDOS is 32 times higher than the vacuum level of $\rho\pi c^2/2\omega = 0.25$. The contrast in the LDOS between points inside and outside of the cylinders is of order 5×10^4. However,

#27699 - $15.00 US
Received November 13, 2000; Revised January 09, 2001

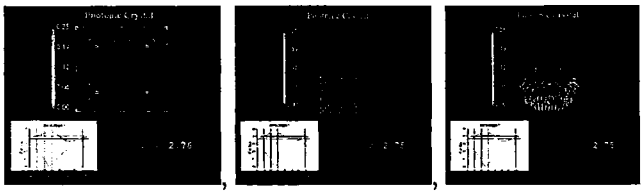

Fig. 5. Quicktime movies of LDOS for TM polarization. Left panel: top.mov (2.49MB) directly from above. Middle panel: above.mov (2.2 MB) from above. Right panel: below.mov (2.4MB) from below.

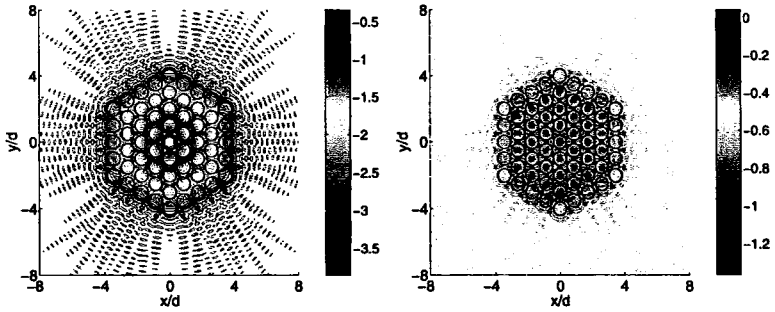

Fig. 6. $\log_{10}(\rho\pi c^2/2\omega n_b^2)$ for TE polarization for $\lambda/d = 2.25$ in a band gap(left panel) and $\lambda/d = 3.0$ in the pass band(right panel).

other wavelengths show enhanced emission from subsets of the cylinders (right panel). From the video clips (see Fig. 5), we see that as the band gap is entered from the short wavelength side, the LDOS initially decreases within the cylinders at the centre of the cluster, gradually evolving into the surrounding matrix. As the wavelength increases, the region of suppressed emission increases and approaches the edge of the cluster. At the long wavelength edge of the gap the high values of the LDOS emerge from inside the cylinders. For wavelengths greater than $\lambda/d = 3.8$, there is oscillatory character in the LDOS and, while the physics of this behavior is not yet clear, it is likely to be associated with Fabry-Perot interference effects between layers, or with resonances of, or between, individual cylinders. Some further investigation of this appears necessary.

For TE polarization, it is possible to form a band gap with air cylinders in a dense, homogeneous matrix [15] and to generate a full band gap with a hexagonal array. Figure 6 shows the LDOS for TE polarization with dense hexagonally packed voids ($n_l = 1$) with radii $a/d = 0.48$ in a high index matrix ($n_b = \sqrt{13}$) for both pass band and gap wavelengths. For this geometry, the LDOS exhibits six-fold symmetry (rather than four-fold symmetry of previous examples), together with strong interference and diffraction effects. We note further that for TE polarization the LDOS is discontinuous at the cylinder surfaces, whereas for TM polarization it is continuous.

In conclusion, we examine properties of the LDOS for 2D photonic crystals, in both band gaps and pass bands and show far reaching control over the radiation dynamics of a line source. For example, inside a cylinder cluster the LDOS decreases exponentially in a band gap and exhibits oscillatory behavior in a pass band. On the long wavelength edge of the gap, the spatial distribution of LDOS may vary by factors of order 10^4 and, indeed, the video clips show complex and interesting behavior that merits further investigation.

We acknowledge financial support from the Australian Research Council and thank Sajeev John and John Sipe for useful discussions. KB acknowledges support by the Deutsche Forschungsgemeinschaft under Grant No. Bu 1107/2-1.

#27699 - $15.00 US
Received November 13, 2000; Revised January 09, 2001